Novel Use of an Internal Mercury-Argon Lamp for the Calibration of Raman Wavenumber, Bandwidth, and Relative Intensities in Large Raman Images of Astromaterials.

Ryan S. Jakubek[1] and Marc D. Fries[2], [1]Jacobs JETS Contract, NASA-JSC, Houston, Texas 77058, USA, [2]NASA Johnson Space Center, Mailcode XI2, 2101 NASA Parkway, Houston, TX 77058, USA. Email: ryan.s.jakubek@nasa.gov

Introduction: Raman imaging is an emerging tool for the analysis of astromaterials, as it is capable of describing mineralogy[1–6], crystal orientation[3,7], and mineral composition as well as carbon composition/speciation[8–10] and thermal history[11–17] all within a petrographic context. Adequately examining the heterogeneous composition of a meteorite, while maintaining low laser powers needed to prevent damage to meteorite mineralogy and organics, often requires the collection of large Raman images with long collection times on the timescale of days. However, the wavenumber, relative Intensity, and bandwidth calibration of the Raman instrument/spectrometer drifts on long timescales[18,19] resulting in low precision for the Raman spectra comprising a large Raman image. This decrease in wavenumber, bandwidth, and relative intensity precision is a source of error which can compromise the analysis of geological markers that can provide important information on a meteorite sample. Examples of measurements which require accurate resolution on the scale of single wavenumbers include mineral composition and carbon microstructure. We examine, in detail, the change in bandwidth, relative intensity, and wavenumber of the Raman bands and Hg-Ar emission lines in our Raman images as a function of time and laboratory temperature.

To overcome drifts in calibration, we utilize a commercial WITec Raman instrument with an internal Hg-Ar calibration lamp to individually calibrate each spectrum in the Raman image.[20,21] Our instrument, known as "Ratatoskr", uses a beam splitter in place of the customary mirror to facilitate collection of Hg-Ar calibration lines concurrent with Raman spectra. This allows collection of calibration lines with each spectrum within the Raman image, as opposed to performing calibrations before and/or after a measurement. We show that using the internal calibration we can improve the wavenumber, relative intensity, and bandwidth precision for the spectra in our Raman images, which were collected over multiple days. For example, our recent paper demonstrates an improvement in peak position precision from ±0.15 to ±0.05 cm^{-1}. This is important as it improves measurements of mineral chemistry, latent strain, and other features that are dependent upon accurate peak position determination. In our work we suggest general methods for calibrating the wavenumber, relative intensity, and bandwidth of Raman spectra in large Raman images. Adoption of these techniques in the astromaterials community will improve the scientific rigor of measurements performed in individual laboratories as well as improving the comparability of results reported in different laboratories. This improvement will be especially important for reporting results from sample return missions such as OSIRIS-REx Hayabusa, Hayabusa2, and Mars Sample Return where Raman measurements such as carbon microstructure require sub-cm^{-1} precision in both position and bandwidth [2,8,9,15–17,22–24].

Instrumentation: Our Raman internal calibration is performed using the "Ratatoskr" WITec α300R confocal Raman microscope (XMB3000-3003) used by NASA Curation for collections support. The instrument contains a Hg-Ar emission lamp that is integrated into the optical path of the collected Raman scattering using a beam splitter. The Hg-Ar calibration lines and Raman scattered light are simultaneously sent to the spectrometer along the same optical path. This configuration allows for the Hg-Ar calibration lines to be observed in every spectrum when collecting Raman microscopy images over long periods of time. Figure 1 shows an optical diagram of the instrumentation.

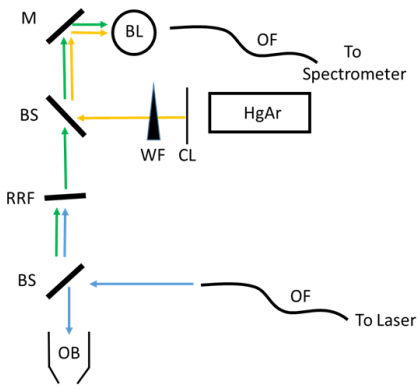

Figure 1: Optical diagram of Raman microscope with internal calibration lamp. The labels in the figure are as follows: M = mirror, BS = beam splitter, RRF = Rayleigh rejection filter, OB = objective, WF= wedge filter, CL= collimating lens, Hg-Ar = mercury argon lamp, BL = ball lens, and OF = optical fiber. The blue arrows, green arrows, and orange arrows indicate the optical path of the incident laser light, the Raman scattered light, and the Hg-Ar lamp light, respectively.

Novel Calibration Technique and Comparison to Existing Methods: The standard technique used for the calibration of Raman images is to regularly collect a spectrum of a Raman standard material or emission lamp, placed at the sample position, before image collection.[13] However, changes in environmental and instrumental conditions cause the calibration to drift with time.[19,25] This results in a shift in observed Raman band peak wavenumbers, relative intensities, and bandwidth throughout the collection of a Raman image. These drifts cannot be accounted for using the standard calibration techniques because Raman image collection would be interrupted when collection a calibration spectrum.

By using a beam splitter to direct light from a Hg-Ar calibration lamp along the same optical path as the Raman scattered light (Figure 1), we are able to calibrate wavenumber and bandwidth for each individual Raman spectrum within a Raman image eliminating the observed temporal calibration drift. Spectral calibration is performed for every spectrum in a Raman image through post-processing. After calibration, peak relative intensity, position, and width are known to high precision and can be compared across measurements collected on different instruments.

As stated above, calibration of all spectra in a Raman image is performed in post-processing. For peak wavenumber calibration, each Raman spectrum is calibrated from the known peak wavenumbers of the Hg-Ar lamp lines using a linear cm^{-1}/pixel calibration. For bandwidth calibration the widths of the Hg-Ar lines approximate the spectrometer slit function of the instrument allowing one to deconvolve the Gaussian slit function from observed Raman band for every band in each Raman spectrum. For relative intensity, we utilize the relative intensity of the Hg-Ar lines to determine the instrument response function of the instrument. Thus, for each spectrum we can estimate the instrument response function for the entire spectral wavenumber range and calibrate relative intensities.

Calibration Improves Mineralogical and Organic Calculation Precision: The improvement of Raman wavenumber, relative intensity, and bandwidth precision in our Raman images accounts for errors arising from thermal and other sources of calibration drift during long Raman scans. It also facilitates cross-laboratory analyses and data reporting by allowing a standardized method for Raman image calibration. Additionally, it supports future work into generating modal abundance and other calculations from Raman images in a scientifically robust fashion. To demonstrate this, we determined the expected error in the calculation of olivine forsterite number from the frequency shift of the DB2 Raman band.[22–24] We show that calibrating each Raman spectrum individually in our Raman images decreases the error in the calculated forsterite number by ~59% [20]. Thus, our calibration technique can significantly decrease systematic error in Raman images of astromaterials..

Acknowledgments: Funding for this work was provided as an Advanced Curation project run by the NASA Astromaterials Acquisition and Curation Office, Johnson Space Center.

References:

[1] McMillan, P. F. *Annu. Rev. Earth Planet. Sci.* **17**, 255–279 (1989). [2] Wang, A., et. al. *J. Raman Spectrosc.* **35**, 504–514 (2004). [3] Fries, M. & Steele, A. in *Confocal Raman Microscopy* 111–135 (Springer, 2010). [4] Ling, Z. C., Wang, A. & Jolliff, B. L. *Icarus* **211**, 101–113 (2011). [5] Lafuente, B., Downs, R. T., Yang, H. & Stone, N. *Gruyter, Berlin, Ger.* **1**, 30 (2015). [6] Steele, A. *et al. Meteorit. Planet. Sci.* **42**, 1549–1566 (2007). [7] Maxfield, J., Stein, R. S. & Chen, M. C. *J. Polym. Sci. Polym. Phys. Ed.* **16**, 37–48 (1978). [8] Pasteris, J. D. & Wopenka, B. *Can. Mineral.* **29**, 1–9 (1991). [9] Wopenka, B. & Pasteris, J. D. *Am. Mineral.* **78**, 533–557 (1993). [10] Ferrari, A. C. & Robertson, J. *Phys. Rev. B* **61**, 14095 (2000). [11] Beyssac, O., et al. *Contrib. to Mineral. Petrol.* **143**, 19–31 (2002). [12] Beyssac, O., Goffé, B., Chopin, C. & Rouzaud, J. N. *J. Metamorph. Geol.* **20**, 859–871 (2002). [13] Cody, G. D. *et al. Earth Planet. Sci. Lett.* **272**, 446–455 (2008). [14] Visser, R., et al. *Geochim. Cosmochim. Acta* **241**, 38–55 (2018). [15] Bonal, L., Quirico, E., Bourot-Denise, M. & Montagnac, G. *Geochim. Cosmochim. Acta* **70**, 1849–1863 (2006). [16] Bonal, L., et al. *Geochim. Cosmochim. Acta* **71**, 1605–1623 (2007). [17] Bonal, L., et al. *Geochim. Cosmochim. Acta* **189**, 312–337 (2016). [18] Mestari, A., Gaufrès, R. & Huguet, P. *J. Raman Spectrosc.* **28**, 785–789 (1997). [19] Fukura, S., Mizukami, T., Odake, S. & Kagi, H. *Appl. Spectrosc.* **60**, 946–950 (2006). [20] Jakubek, R. S. & Fries, M. D. *J. Raman Spectrosc.* (2020). [21] Jakubek, R. S., Fries, M. D. *J. Raman Spectrosc.* (2020). [22] Kuebler, K. E., et al. A. *Geochim. Cosmochim. Acta* **70**, 6201–6222 (2006). [23] Welzenbach, L. C. in *79th Annual Meeting of the Meteoritical Society* vol. 1921 (2016). [24] Pittarello, L., et al. *Meteorit. Planet. Sci.* **50**, 1718–1732 (2015). [25] Odake, S., Fukura, S. & Kagi, H. *Appl. Spectrosc.* **62**, 1084–1087 (2008).